

MODELLING OF THE PRE-ARCING PERIOD IN HBC FUSES INCLUDING SOLID - LIQUID - VAPOUR PHASE CHANGES OF THE FUSE ELEMENT

D. Rochette¹, W. Bussière², R. Touzani³, S. Memiaghe², G. Velleaud¹ and P. André²

¹ Laboratoire Arc Electrique et Plasmas Thermiques, CNRS UMR 6069, IUT de Montluçon, avenue Aristide Briand 03101 Montluçon, France.

rochette@moniu.univ-bpclermont.fr, velleaud@moniu.univ-bpclermont.fr.

² Laboratoire Arc Electrique et Plasmas Thermiques, CNRS UMR 6069, Université Blaise Pascal, 24 avenue des Landais, 63177 Aubière, France.

william.bussiere@univ-bpclermont.fr, steeve.memiaghe@univ-bpclermont.fr, pascal.andre@univ-bpclermont.fr

³ Laboratoire de Mathématiques, CNRS UMR 6620, Université Blaise Pascal, 24 avenue des Landais 63177 Aubière, France.

rachid.touzani@univ-bpclermont.fr.

Abstract: In this paper, we present a model and a numerical method of the fuse element heating including solid - liquid - vapour phase transitions in order to evaluate the pre-arcing time in HBC fuses. The mathematical model is based on the enthalpy formulation of the heat equation with a source term representing the Joule effect coupled with the Laplace equation for the potential and the Ohm's law. We obtain an approximation of the governing equations using a specific numerical scheme for time discretization and unstructured triangle or tetrahedral element grids are employed in spatial discretization using a standard piecewise linear finite element method. Numerical simulations of two fuse elements, used in industrial applications, are carried out and compared with experimental measurements obtained using a 100 kVA power station.

Keywords: Pre-arcing time, 3D Thermal/Electric model, Finite element method, Phase change.

1. Introduction

Numerous numerical investigations can be found in the literature on the study of the fuse pre-arcing regime [1-6] in order to evaluate the time/current characteristics and to be a useful tool for the fuse element design. This work relating once again to the study of the pre-arcing period in High Breaking Capacity (HBC) fuses is motivated by the aim at developing in future works a physical model of the fuse operation, *i.e.* pre-arcing and arcing models. To ensure the transition between the two regimes, we must extend the fuse element heating by Joule effect until vapour phase appears, *i.e.* initiation of the electric arc.

For this purpose, we have developed a 3D-model of the Joule heating of the fuse element. We use a set of equations coupling the thermal and the electrical

phenomena and the solid - liquid - vapour phase transitions are included using an enthalpy formulation. The physical parameters of the silver fuse element depending on the temperature are used. For the short pre-arcing times, we assume no heat transfer between the fuse element and the surrounding porous medium and for medium pre-arcing times, the heat exchanges with the porous medium are prescribed using appropriate boundary conditions. The model and the numerical method are tested with two fuse elements provided with one reduced section. Numerical results for short and medium pre-arcing times are compared with experimental measurements acquired using a 100 kVA power station.

2. Mathematical model

In a simplified approach, the study consists in modelling only the fuse-element where boundary conditions are supplemented to take into account the heat transfer, conductive and radiative, toward the porous medium. Consequently, no information is available on the porous environment.

We have tested two fuse elements provided with only one reduced section. The characteristics of the fuse element 1 are shown in Fig. 1. This one is used to test short pre-arcing time, consequently, we neglect heat transfer toward the porous medium and so a 2D-model is sufficient to describe the phenomenon.

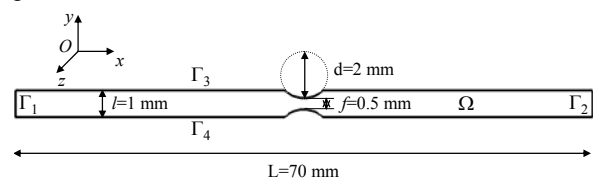


Fig. 1: 2D-geometry of the fuse element 1 of thickness $e = 0.105 \text{ mm}$.

Fig. 2 represents the 3D-geometry of the fuse element 2. This one is tested in the case of the medium pre-arcing time (> 10 ms) where heat exchanges between the fuse element and the porous medium are taken into account using boundary conditions on Γ .

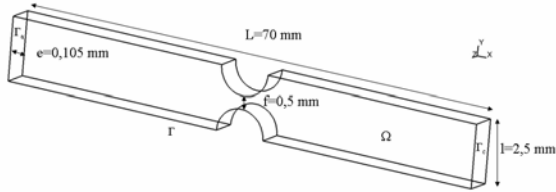


Fig. 2: 3D-geometry of the fuse-element 2.

The fundamental partial differential equation governing the transient Joule heating of the silver fuse element is described by the balance of energy:

$$\frac{\partial H}{\partial t} - \nabla \cdot (k \nabla T) = \frac{|\mathbf{J}|^2}{\sigma} \quad (1)$$

where T is the temperature field, H is enthalpy per unit volume, k and σ are respectively the thermal and electrical conductivities of the silver, all depending on temperature. \mathbf{J} denotes the vector of current density obtained in solving the Laplace equation and the Ohm's law:

$$\begin{cases} \nabla \cdot (\sigma \nabla V) = 0 \\ \mathbf{E} = -\nabla V \\ \mathbf{J} = \sigma \mathbf{E} \end{cases} \quad (2)$$

where V is the electric potential and \mathbf{E} is the electric field vector.

The enthalpy function versus temperature [7], illustrated in Fig. 3, is defined by the general form:

$$H(T) = \int_{T_{ref}}^T \rho c(s) ds \quad (3)$$

with

$$H(T) = \begin{cases} \int_{T_{ref}}^T \rho c(s) ds & \text{if } T < T_m \\ \int_{T_{ref}}^{T_m} \rho c(s) ds + \rho L_m & \text{if } T = T_m \\ \int_{T_{ref}}^{T_m} \rho c(s) ds + \rho L_m + \int_{T_m}^T \rho c(s) ds & \text{if } T > T_m \\ \int_{T_{ref}}^{T_m} \rho c(s) ds + \rho L_m + \int_{T_m}^{T_v} \rho c(s) ds & \text{if } T = T_v \\ \int_{T_{ref}}^{T_m} \rho c(s) ds + \rho L_m + \int_{T_m}^{T_v} \rho c(s) ds + \rho L_v & \text{if } T > T_v \end{cases} \quad (4)$$

where ρ is silver density [8], c is specific heat depending on temperature and T_{ref} is a reference temperature. L_m and L_v denote respectively the melting and boiling latent heats. T_m and T_v are respectively the melting and the boiling temperatures of silver. Notice that multivalued function (4) takes into account phase changes at temperature T_m (solid \rightarrow liquid) and T_v (liquid \rightarrow vapour) of the silver fuse element.

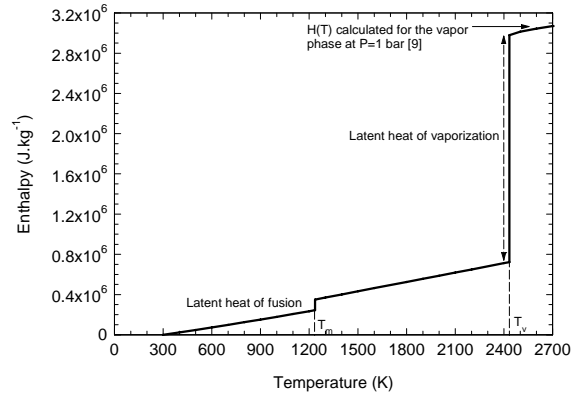


Fig. 3: Enthalpy versus temperature for silver [7].

To solve the transient electric-thermal problem, equations (1) and (2) must be supplemented by initial and boundary conditions.

The initial temperature is fixed at the value $T_0 = 300$ K and we impose the following boundary conditions:

- On boundary Γ_a (*i.e.* anode), we impose the current density flux through the fuse cross section $|\Gamma_a|$:

$$\sigma \frac{\partial V}{\partial \mathbf{n}} = \frac{I(t)}{|\Gamma_a|} \quad (5)$$

where \mathbf{n} is the outward unit normal to the boundary and $I(t)$ is the prospective current of the circuit as described hereafter (see equation (11)).

- On boundary Γ_c (*i.e.* cathode), a reference potential is prescribed $V = 0$.
- On boundary Γ , representing the other boundaries of the fuse element surrounded by silica sand, we have used two heat transfer conditions as:

$$k \frac{\partial T}{\partial \mathbf{n}} = k_{eff} \frac{(T - T_0)}{L} + \varepsilon \sigma_s (T^4 - T_0^4): \text{3D-model} \quad (6)$$

$$k \frac{\partial T}{\partial \mathbf{n}} = 0: \text{2D-model}$$

where k_{eff} is the thermal conductivity of the porous medium, $\varepsilon(T)$ is the silver emissivity, σ_s is the Stefan constant and L is the porous medium length. The first expression assumes that the porous medium is transparent (optically thin) and the second expression assumes no heat transfer.

The principal Silver properties used in the calculations are depicted in Table 1.

Table 1: Silver properties

Density (kg.m^{-3})	$\rho = 10490 \text{ kg.m}^{-3}$
Melting temperature	$T_m = 1235 \text{ K}$
Boiling temperature	$T_v = 2433 \text{ K}$
Latent heat of fusion	$L_m = 1.05 \times 10^5 \text{ J.kg}^{-1}$
Latent heat of boiling	$L_v = 2.26 \times 10^6 \text{ J.kg}^{-1}$

The thermal [10] and electric [11] conductivities depending on temperature are plotted in Fig. 4. For both, the ratio of thermal and electric conductivities at the melting temperature is slightly higher than 2.

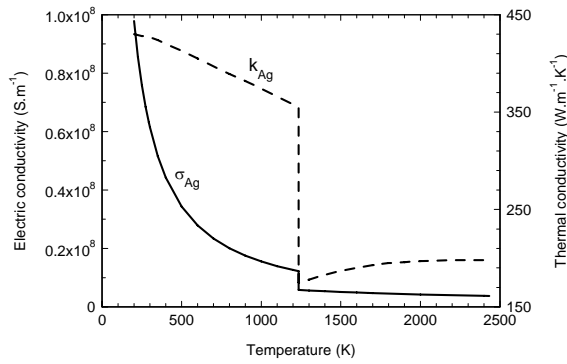


Fig. 4: Thermal [10] and electric [11] conductivities of Silver.

The total hemispherical emissivity of the silver fuse element is obtained by the formulation proposed by Parker and Abbott (Fig. 5):

$$\varepsilon(T) = 0.766 \sqrt{\frac{T}{\sigma}} - \left[0.309 - 0.0889 \ln\left(\frac{T}{\sigma}\right) \right] \left(\frac{T}{\sigma}\right) - 0.0175 \left(\frac{T}{\sigma}\right)^{3/2} \quad (7)$$

with T in K and σ in S.cm^{-1} .

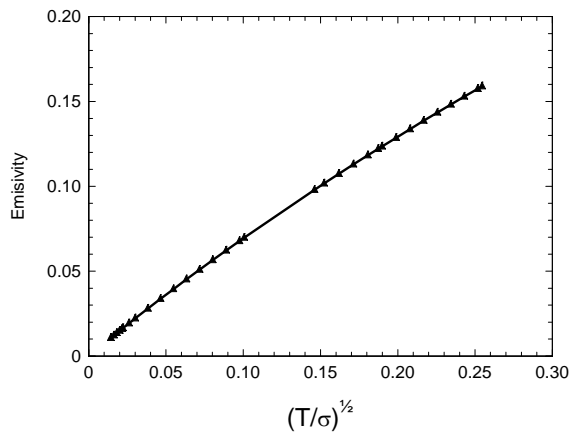


Fig. 5: Total hemispherical emissivity of Silver in function of $\sqrt{(T/\sigma)}$.

3. Numerical solution of the transient heat transfer and the steady potential equation

To obtain an approximation of equations (1)-(4), we consider space discretization by a standard piecewise linear finite element method and for time discretization we use a dedicated scheme for phase transition named ‘‘Chernoff scheme’’ [12]. The so called Chernoff scheme consists in a relaxation of the discontinuous relation enthalpy-temperature (Fig. 3) at the phase change temperatures (*i.e.* melting and boiling temperatures).

Let Δt denote the time step, and H^n , J^n , k^n and σ^n the approximations of the physical parameters at time t^n . We use the time integration scheme as follows:

$$\begin{aligned} \nabla \cdot (\sigma^n \nabla V^n) &= 0 \\ \mathbf{E}^n &= -\nabla V^n \\ \mathbf{J}^n &= \sigma^n \mathbf{E}^n \end{aligned} \quad (8)$$

$$\gamma \frac{T^{n+1} - \beta(H^n)}{\Delta t} - \nabla \cdot (k^n \nabla T^{n+1}) = \frac{|\mathbf{J}^n|^2}{\sigma^n}$$

$$H^{n+1} = H^n + \gamma (T^{n+1} - \beta(H^n))$$

with boundary conditions described in section 2. $\beta(H)$ is the reciprocal form of equation (3) and γ is a relaxation parameter, required to ensure the scheme stability, and satisfies:

$$0 \leq \gamma \leq \frac{1}{\max \beta'(H)} \quad (9)$$

The space discretization of equations (1)-(2) is made by a standard finite element method. Finite element approximation of the system (8) can be summarized as follows: We first consider a triangulation (finite element mesh) of the domain occupied by the fuse element Ω . We consider arbitrary continuous piecewise linear test functions ϕ and ψ and solve the variational system of equations:

$$\begin{aligned} \int_{\Omega} \sigma^n \nabla V^n \cdot \nabla \psi \, d\Omega &= \frac{I(t)}{|\Gamma_a|} \int_{\Gamma_a} \psi \, d\Gamma_a \\ \frac{\gamma}{\Delta t} \int_{\Omega} (T^{n+1} - \beta(H^n)) \phi \, d\Omega + \int_{\Omega} k^n \nabla T^{n+1} \cdot \nabla \phi \, d\Omega &= \int_{\Omega} |\nabla V^n|^2 \phi \, d\Omega \\ H^{n+1} &= H^n + \gamma (T^{n+1} - \beta(H^n)) \end{aligned} \quad (10)$$

Note that we have kept the same notation for the exact and the approximate solution.

Problem (10) can then be written in the form of two linear systems of equations involving symmetric positive definite systems that we solve by a preconditioned conjugate gradient method at each time step n .

4. Experimental power supply

The experimental power supply is built from a single-phase transformer with a 100 kVA true power [13] and the prospective current delivered is given by:

$$I_p(t) = \frac{\hat{V}}{\sqrt{R^2 + L^2\omega^2}} \left(\sin(\omega t + \theta - \varphi) - \sin(\theta - \varphi) \exp\left(-\frac{R}{L}t\right) \right) \quad (11)$$

where \hat{V} is the supply voltage, R is the resistive load, L is the inductive load, ω is the pulsation at 50 Hz, θ is the closing angle, $\cos\varphi$ is the power factor, t is the time. The characteristics of the three experimental tests are given in Table 2. The fuse element 1 is tested to short pre-arcing times with two characteristic closing angles θ . The fuse element 2 is used to obtain medium pre-arcing time.

Table 2: Experimental test characteristics.

	Fuse 1 test 1	Fuse 1 test 2	Fuse 2 test 3
\hat{V} (V)	284.0	284.0	292.6
R (Ω)	0.52	0.54	1.07
L (μ H)	655	582	830
$\cos\varphi$	0.93	0.95	0.97
θ	84°	104°	0°
$I_{p,max}$ (A)	503.6	496.0	265.6

5. Numerical results and experimental recordings

We have performed two experimental tests with the fuse element 1 described in Fig. 1 and one test with the fuse element 2 illustrated in Fig. 2. In this section, we present and compare numerical results to the measurements.

5.1. Fuse element 1 – Test 1

Fig. 6 gives recordings of the electrical parameters of the test 1, *i.e.* evolutions of the prospective current, the fuse current, the supply voltage and the fuse voltage during the fuse operation and the simulated current.

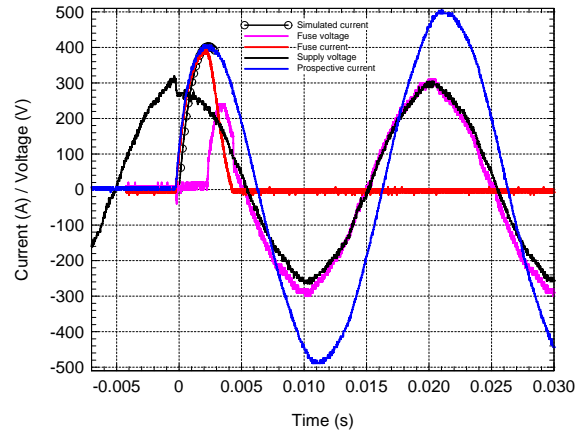


Fig. 6: Prospective and fuse current, supply and fuse voltage recordings and the simulated current during the test 1 for a power factor $\cos\varphi = 0.93$ and a closing angle $\theta = 84^\circ$.

The experimental pre-arcing time is evaluated at $t_{prearc} = 2.5 \text{ ms}$ and the arcing time around $t_{arc} = 2.2 \text{ ms}$. The fault current is interrupted at the middle of the first half 50 Hz-period. When the current is returned to zero, the voltage across the fuse reaches the supply voltage.

For numerical simulation, we use the 2D-model because we assume no heat transfer toward the porous medium for the pre-arcing times considered. The fuse element is discretized with an unstructured mesh of 12076 triangles and 6609 nodes where the reduced section is meshed more finely. At the initial time, the temperature is fixed at the ambient temperature and the time step is prescribed at $\Delta t = 10^{-5} \text{ s}$ in order to visualize the two constant stages of temperature. For all the simulations, we stop the calculation when the enthalpy of vaporization is reached.

Fig. 7 and 8 present the numerical results of the test 1 using the fuse element 1.

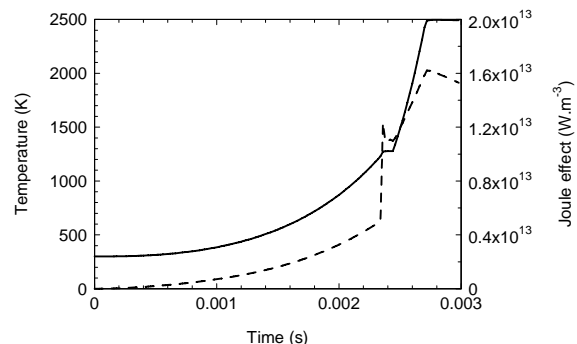


Fig. 7: Temperature (solid line) and Joule effect (dashed line) histories at the reduced section centre ($x = 35 \text{ mm}$, $y = 0.5 \text{ mm}$) during the pre-arcing time.

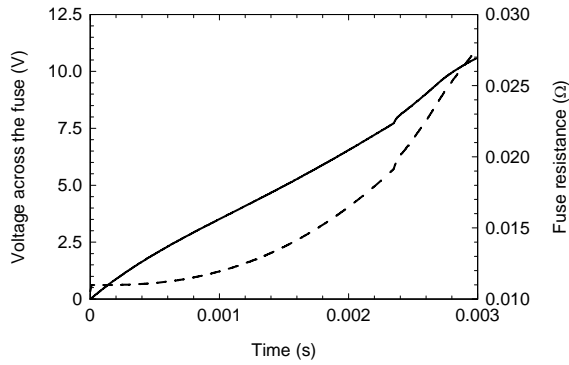


Fig. 8: Voltage across the fuse (solid line) and fuse resistance (dashed line) evolutions during the pre-arcing time.

The pre-arcing time simulated is about 3 ms compared to the 2.5 ms obtained by measurements. The temperature evolution can be divided in four steps:

- A gradual increase up to the melting temperature due to the Joule heating.
- A time lapse corresponding to the solid - liquid phase transition during which the melting latent heat energy is brought. We observe a discontinuous jump of the Joule effect due to the drop of the electric conductivity in liquid phase. The peak observed on the Joule effect curve is a numerical effect without physical explanation.
- An important temperature rise due to the maximum current density and the high resistivity of the fuse element.
- A time range carried out at constant boiling temperature during which liquid - vapour phase change occurs until the vaporization enthalpy is reached.

5.2. Fuse element 1 – Test 2

Fig. 9 gives the electrical parameters of the test 2 carried out with the fuse element 1.

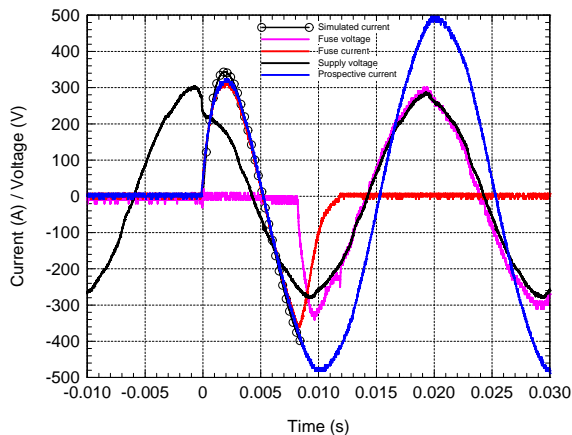


Fig. 9: Prospective and fuse current, supply and fuse voltage recordings and simulated fuse current during the experimental fuse test 2 for a power factor $\cos\varphi = 0.95$ and a closing angle $\theta = 104^\circ$.

The experimental pre-arcing time is evaluated at $t_{prearc} = 8.3\text{ms}$ and the arcing time around $t_{arc} = 4\text{ms}$. The fault current is interrupted at the second half 50 Hz-period.

Fig. 10 and 11 present the 2-D model numerical results carried out with the fuse element 1 and the characteristics of the test 2.

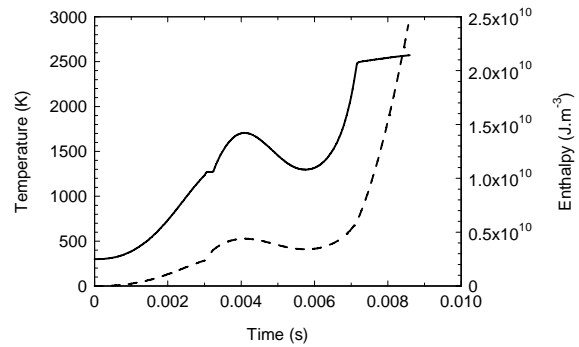


Fig. 10: Temperature (solid line) and enthalpy (dashed line) histories at the notch centre during the pre-arcing time.

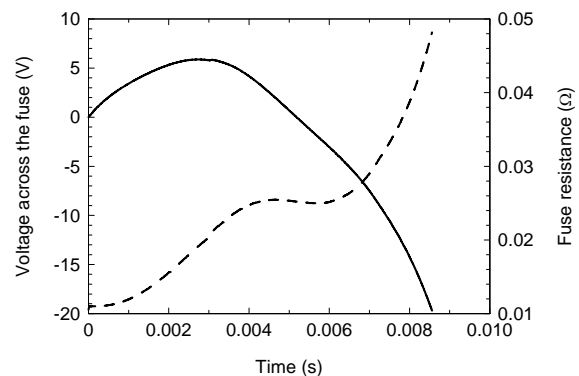


Fig. 11: Voltage across the fuse and fuse resistance evolutions during the pre-arcing time.

The simulated pre-arcing time is evaluated around 8.5 ms in agreement with the measured pre-arcing time. The shape of the temperature curve differs from the test 1. The melting stage of the temperature is clearly visible around 3 ms without an electric arc being initiated. Next, the temperature increases and decreases due to the combination of the Joule effect and the conduction heat transfer. Indeed, when the current return to zero, only heat transfer by conduction exists and the heat flow cools the hot area (reduced section) and heats the cold area (fuse ribbon). During the negative half-wave (Fig. 9), the Joule effect is sufficient to reach the vaporization enthalpy. We note in Fig. 11 that the fuse resistance gradually increases. Indeed, the notch temperature decreases but the heat energy is transferred to the fuse strip.

5.3. Fuse element 2 – Test 3

Fig. 12 gives the electrical parameters of the test 3 using the fuse element 2.

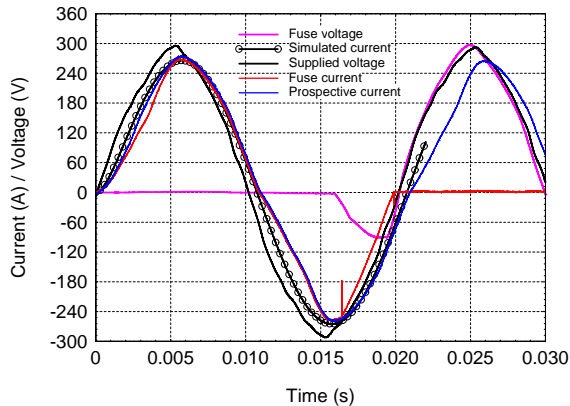


Fig. 12: Prospective and fuse current, supply and fuse voltage recordings and simulated current during the experimental fuse test 3 for a power factor $\cos\varphi = 0,97$ and a closing angle $\theta = 0^\circ$.

The pre-arcing time obtained by measurements is 16.5 ms and the arcing period is around 3.5 ms. The simulations have been performed with the 3D-model to take into account heat exchanges between the fuse element and the porous medium. In order to obtain reasonable computational times, we have simulated only one quarter of the fuse geometry and the time step is fixed at $\Delta t = 2 \cdot 10^{-5} s$. The fuse element is discretized with tetrahedral cells.

Fig. 13 shows isothermal contours in the fuse element close to the reduced section at the end of the pre-arcing time *i.e.* 22 ms. The temperature distribution is almost homogeneous in the fuse ribbon. As expected, the notch temperature is close to the boiling temperature.

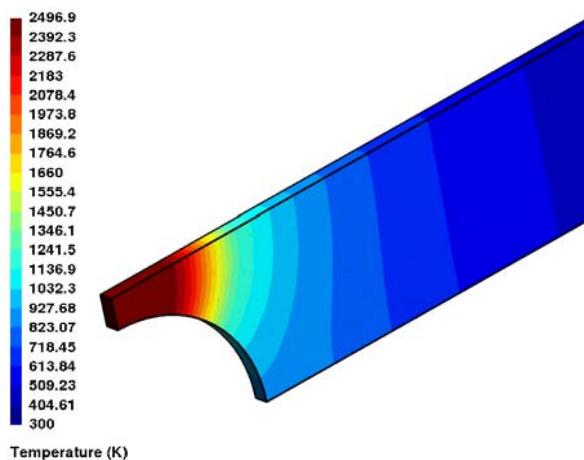


Fig. 13: Temperature distribution in the fuse element 2 at time $t = 22 ms$.

Fig. 14 represents the temperature evolution at the notch centre of fuse element 2 during medium pre-arcing.

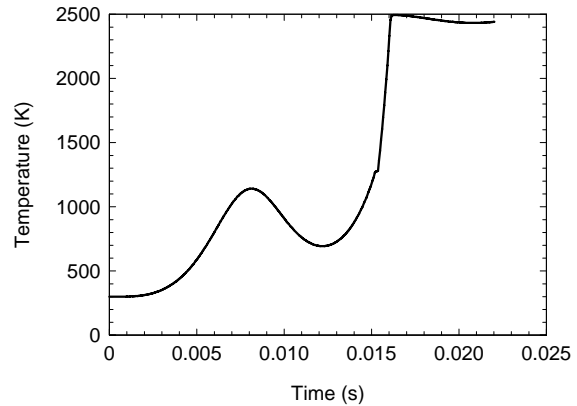


Fig. 14: Temperature evolution at the notch centre with conduction/radiation heat transfers between fuse element and the porous medium.

The simulated pre-arcing time is 22 ms compared to the 16.5 ms obtained by experiment. We have realized the same simulation without heat exchanges toward the porous medium and we have obtained a similar pre-arcing time.

6. Discussion and conclusion

The discrepancies observed between experiments and simulations pre-arcing times ($t_{pre-arc}^{experiment} > t_{pre-arc}^{simulation}$) can be explained as follows:

- By a microscopic visualization, we have observed that the real fuse element was not perfectly symmetric on the level of the reduced section.
- Silver electric conductivities of [11] are given until 1700 K in the liquid phase. So, we have extrapolated data until the boiling temperature. Moreover, when the boiling temperature is reached, the boiling stage temperature is rather long and during this stage the electric conductivity $\sigma(T_v)$ is constant. A significant drop of the electric conductivity probably happens during the contribution of the boiling latent heat.

In our opinion, these results must be taken with precaution. Indeed, it is surprising that the liquid phase in test 2 (Fig. 10) lasts also a long time (around 5 ms). An experimental measure which could be useful to validate the temperature evolution of Fig. 10 (the liquid phase lasts 5 ms) would be to measure with precision the voltage across the fuse during the pre-arcing time. Indeed, in liquid phase the fuse resistance increases significantly (Fig. 11) influencing the voltage across the fuse.

In spite of these remarks, the model allows to extend the pre-arcing time calculation until the vapour phase appears and from this moment a coupling with a gas flow model in porous medium would allow to investigate the beginning of the arcing period.

Acknowledgments

We thank for their financial support MM. T. Rambaud and JL. Gelet from Ferraz Shawmut, M. F. Gentils from Schneider Electric, and M. JC. Perez-Quesada from Mesa.

References

- [1] J.G. Leach, P.G. Newbery, A. Wright, Analysis of high-rupturing-capacity fuslink prearcing phenomena by a finite-difference method, *Proceedings of the IEE*, vol. 120, n°9, September, 987-993, 1973.
- [2] M.S. Agarwal, A.D. Stokes and P. Kovitya, pre-arcing behaviour of open fuse wire *J. Phys. D: Appl. Phys* 20, 1237-1242, 1987.
- [3] C. Garrido and J. Cidras, a method for predicting time-current characteristics of fuselinks, *Electric Machines and Power Systems*, 26: 685-698, 1998.
- [4] Y. Kawase, T. Miyatake, and S. Ito, Heat Analysis of a Fuse for Semiconductor Devices Protection Using 3-D Finite Element Method, *IEEE Transactions on Magnetics*, vol. 36, no.4, July 2000.
- [5] P.M. McEwan and R. Wilkins, A decoupled method for predicting time/current characteristics of H.R.C. fuses. Proceedings of ICEFA, Liverpool Polytechnic, 33-41, 1976.
- [6] A. Wright and P.G. Newberry, *Electric Fuses*, 3rd Edition, IEE Power & Energy series 49., 2004.
- [7] Bahrin, *Thermochemical Data of Pure Substances*, 3rd ed. in collaboration with G. Platzki, vol. 1. Ag-Kr and vol. 2. La-Zr, VCH Weinheim, Federal Republic of Germany, New York, 1995.
- [8] L-D. Lucas, Densité des principaux métaux et métalloïdes, *Techniques de l'ingénieur, Matériaux métalliques*, M. 65, MB. 2, in French, 1984.
- [9] D. Rochette, W. Bussière, P. André, Composition, enthalpy and vaporization temperature calculation of Ag-SiO₂ plasmas with air in the temperature range from 1000 to 6000 K and for pressure included between 1 to 50 bars, *Plasma Chemistry and Plasma Processing*, vol. 24, n°3, 475-491, 2004.
- [10] Y.S. Touloukian, *Thermal conductivity: metallic elements and alloys*, Series technical ed. IFI/Plenum New York Washington, 1970.
- [11] R.A. Matula, Electrical Resistivity of Copper, Gold, Palladium, and Silver *JPCRD* 8(4), 1147-1298, 1979.
- [12] A.E. Berger, H. Brézis and J.C.W. Rogers, A numerical method for solving the problem $u_t - \Delta f(u) = 0$, *R.A.I.R.O. Numerical analysis* 13 (4) 297-312, 1979.
- [13] W. Bussière, D. Rochette, C. Achard, P. André, T. Latchimy, A. Lefort and G. Velleaud, *Séminaire sur les Fusibles Moyenne Tension, SFMT* February 2006, <http://hal.archives-ouvertes.fr/hal-00019683> (in French).